J Appl Electrochem (2013) 43:1197–1206
DOI 10.1007/s10800-013-0607-5

RESEARCH ARTICLE

Numerical study of ionic current rectification through non-uniformly charged micro/nanochannel systems

Reiyu Chein · Bogan Chung

Received: 10 May 2013 / Accepted: 5 August 2013 / Published online: 18 August 2013

Abstract Ionic transport through cylindrical nanochannels with linearly varied surface charge density was numerically investigated. The ends of the nanochannel were connected to microchannels regarded as reservoirs. The walls at the micro/nanochannel junction were referred to as sidewalls that can be electrically neutral or charged. The results showed that the charged sidewalls could enhance the concentration polarization compared to neutral sidewalls. For neutral sidewall, a limiting current similar to charged permselective membranes and a maximum current rectification ratio at certain bulk concentration similar to charged conical nanopores can be found. For the charged sidewall case, no limiting current regime can be observed and the current varied linearly with the applied voltage with a larger slope compared to the Ohmic relation regime. Moreover, no maximum current rectification ratio can be found and the current rectification ratio increased with the decrease in bulk concentration and increases in surface charge density and sidewall length.

Keywords Micro/nanochannel junction · Charged sidewall · Linearly varied surface charge density · Limiting current · Current rectification

1 Introduction

Nanofluidics is the study of fluid flow in and around nanometer-sized objects with at least one characteristic dimension below 100 nm [1, 2]. It has been determined that the nanochannel high surface-to-volume ratio results in a surface charge-governed ion transport regime with the fixed charge on the nanochannel wall largely responsible for phenomena, such as ion enrichment and depletion [3], ion selectivity [4], and ionic current rectification [5]. These phenomena provide the potential for controlling and manipulating fluids in nanochannels with potential applications, such as analyte preconcentration [6, 7], molecule sensing and separation [8, 9], nanofluidic diodes and transistors [10–13], and energy conversion [14, 15]. It can be expected that more new physical phenomena and applications will be discovered and explored.

Among the nanochannel properties, ionic current rectification has received much attention because of its similarity to the biological behavior of living cells. Ionic current rectification through a nanochannel can be found by having geometric or surface charge asymmetry along the ionic current flow axis. An example of geometric asymmetry is a conical pore that has a nanoscale diameter tip and a larger diameter base [16]. When an electric field is applied such that the counterions travel from the tip to base, the resulting ionic current is higher than when counterion transport is from the base to tip. In surface charge asymmetry, the heterogeneous surface charge density along the channel wall can be produced by coating different materials onto the channel wall [17]. Depending on the applied electric field direction, ions are accumulated or depleted inside the nanochannel. Ion accumulation causes current rectification while ion depletion causes current saturation at a low value. In addition to geometric and surface charge asymmetries, another ionic current rectification mechanism is the asymmetric bulk concentrations in baths connected to the ends of nanochannels [18]. The ionic flux unbalance resulting from an applied electric field produces ionic current rectification.

R. Chein (✉) · B. Chung
Department of Mechanical Engineering, National Chung Hsing University, Taichung 40227, Taiwan
e-mail: rychein@dragon.nchu.edu.tw

The nanochannel is also adopted as a simple model in studying ion-selective membrane characteristics. An important ion transport phenomenon in ion-selective membranes is concentration polarization [19]. With sufficiently high voltage, the ionic current through the membrane exceeds the limiting current predicted by the classical diffusion-limited current transport theory [20]. Below the critical voltage for this limiting current, the current varies linearly with the voltage according to the Ohmic law. With further increase in voltage the current saturates to an almost constant limiting current. The corresponding ionic concentration distribution shows that an electro-neutral diffusion layer with concentration gradient appears near the membrane/electrolyte interface on the anodic side. The concentration gradient increases with the increase in applied voltage. When the ion concentration approaches zero and the concentration drop across the diffusion layer cannot increase further, the current approaches a limiting value. The reason for the over-limiting current in a conductive membrane is a subject of intense discussion in the literature. It has been suggested that fluid mixing destroys the diffusion layer and results in the over-limiting current phenomenon [21, 22]. These studies indicated that fluid mixing shortens the diffusive layer thickness, consequently resulting in high current.

From the practical point of view, the nanochannel must be connected to either reservoirs or microchannels in order to carry out the specific applications. Therefore, the charged condition of the reservoir or microchannel walls becomes one of the factors that affect the ionic transport through a nanochannel. The charged surface at the nanochannel entrance can have similar electrostatic influence on mobile ions as that of the charged nanochannel wall and affect the ion transport through the nanochannel. However, most of the studies on the ionic transport phenomena in nanofluidic devices reported in the literature focused on the nanochannel surface charge effect and paid less attention to the charged entrance effect [23–25]. The numerical results of Aguilella-Arzo et al. [23] showed that the charged entrance can reduce the electric resistance for the current flow because of greater counterion accumulation. Cheng and Guo [24] examined the ionic transport in a straight nanochannel by including the entrance effect. The uniform surface charge density was considered in their study. Kubeil and Bund [25] examined the charge distribution effect at a conical nanopore entrance and showed that the charge distribution has a significant effect on the ionic transport through the pore.

The ionic current rectification studied in the past focused on conical pores with uniformly distributed surface charge density. The studies on the inhomogeneous surface charge density effect on current rectification were relatively few. In addition to nanofabrication techniques for producing the non-uniform surface charge density distributions [17], it should be noted that the non-uniform surface charge density on a nanochannel wall results from a variety of origins ranging from manufacturing defects to the adsorption of impurities onto the wall [26, 27]. In the studies of Ramirez et al. [28] and Kosinska et al. [29], the 1-D model was developed for ionic transport through a nanopore with non-uniform surface charge density distribution. However, the entrance effect was not included. Qian et al. [30] studied the non-uniformly distributed surface charge density effect along a conical pore on ionic current rectification. However, the entrance charged condition effect was not addressed.

This study examines the charged nanochannel entrance and surface charge variation along a straight nanochannel and their effects on the ionic current rectification through the nanochannel. This study is conducted by solving the coupled Poisson–Nernst–Planck and Navier–Stokes equations under various applied voltages. Based on the computed ion concentration distributions, the electric current–voltage relation (I–V curve) can be obtained by computing the ion concentration distributions and identifying the entrance and surface charge density variation effects along the nanochannel.

2 Physical model

We consider a straight cylindrical nanochannel having a length of L and radius of a, as shown in Fig. 1a. Two microchannels with length of L_R and radius of b are connected at the nanochannel ends. These two microchannels can also be regarded as reservoirs. Electrodes are placed at the ends of these two microchannels to provide electrical potential bias across the micro/nanochannel system. The externally applied voltage is denoted as $\Delta\phi = \phi_1 - \phi_2$. The resulting electrical field moves in the positive z direction when $\Delta\phi > 0$ and in the negative z direction when $\Delta\phi < 0$. An aqueous salt solution with a bulk molar concentration of c_0 is assumed to entirely fill the system. The system is in equilibrium when $\Delta\phi = 0$. The nanochannel wall is charged with a surface charge density of σ_{ch}. One of the linearly varied surface charge density distributions used in the study of Ramirez et al. [28] was adopted in this study,

$$\sigma_{ch} = \sigma_{av}\left(1 + 2A\frac{z}{L}\right), \quad (1)$$

where σ_{av} is the averaged surface charge density over the entire nanochannel length, and A is a parameter that specifies the slope of the distribution. Note that the $A = 0$ case corresponds to a uniformly charged nanochannel with surface charge density of σ_{av}.

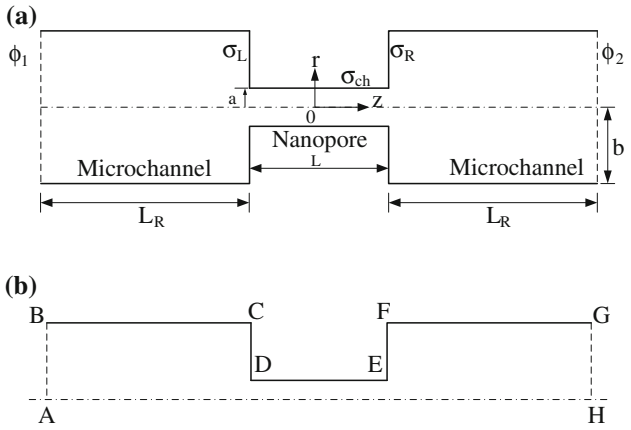

Fig. 1 **a** Schematic diagram of surface-charged straight nanochannel. **b** Computational domain used in two-dimensional modeling

There are two annular sidewalls at the micro/nanochannel junctions as shown in Fig. 1a. As mentioned in the introduction, less attention is paid to the sidewall-charged condition effect on ionic transport through the nanochannel. In order to examine the sidewall charge effect on ion transport, we consider the sidewalls to be either charged or electrically neutral. As shown in Fig. 1a, the surface charge densities of the left and right sidewalls are assigned as σ_L and σ_R, respectively. The remaining microchannel walls are assumed to be uncharged to simplify the analysis. The inclusion of a surface charge along the sidewalls is expected to produce counterion enrichment or depletion in the nanochannel entrance and exit regions. This leads to a decrease or increase in the access resistance and may have a significant effect on the overall ionic current flow through the nanochannel [23–25].

3 Mathematical model

Because the entrance effect cannot be included in the 1-D model, a two-dimensional model is used for analyzing the ionic transport in this study. Ionic flux in the nanochannel is described using the Nernst–Planck equation for each species based on the continuum hypothesis [31],

$$\vec{J}_i = -D_i \nabla c_i + m_i z_i c_i \nabla(\phi + \psi) + \vec{V} c_i, \tag{2}$$

where $\vec{J}_i$, D_i, m_i, c_i, and z_i are the ionic flux, molecular diffusivity, electrical mobility, molar concentration, and charge valance of ith ion, respectively. ϕ is the electrical potential distribution due to the externally applied voltage, and ψ is the potential due to the surface charge density on the wall. ϕ and ψ are described using the Laplace and Poisson equations, respectively,

$$\nabla^2 \phi = 0, \tag{3}$$

$$\nabla^2 \psi = -\frac{\rho_e}{\varepsilon \varepsilon_0}. \tag{4}$$

In Eq. (4), ε is the dielectric permittivity, ε_0 is the permittivity of vacuum, and ρ_e is the space charge density defined as,

$$\rho_e = F \sum_{i=1}^{N} z_i c_i, \tag{5}$$

where F is Faraday's constant and N is the number of ionic species. The ion electrical mobility for dilute electrolytes can be related to the molecular diffusivity D_i using the Nernst–Einstein equation as [31],

$$m_i = \frac{D_i}{RT}, \tag{6}$$

where R is the universal gas constant and T is the fluid temperature. Under steady state with no species generation or destruction source, the ionic flux satisfies,

$$\nabla \cdot \vec{J}_i = 0. \tag{7}$$

In Eq. (2), $\vec{V}$ is the electrolyte flow velocity described using the Navier–Stokes equation,

$$\nabla \cdot \vec{V} = 0, \tag{8a}$$

$$\vec{V} \cdot \nabla \vec{V} = -\nabla p + \mu \nabla^2 \vec{V} - \rho_e \nabla(\phi + \psi), \tag{8b}$$

where p and μ are the pressure and viscosity, respectively. The last term on the right-hand side of Eq. (8b) is known as the electrical body force per unit volume when the electrostriction and permittivity gradient in the electrical field are neglected. After solving Eqs. (2–8) with the appropriate boundary conditions, the current density in the flow field can be calculated as,

$$\vec{i} = -\Lambda \nabla(\phi + \psi) - F \sum z_i D_i \nabla c_i + F \vec{V} \sum z_i c_i, \tag{9}$$

where $\Lambda = F^2 \sum z_i^2 m_i c_i$ is the electrolyte electrical conductivity. The total current through the nanochannel can be obtained by integrating Eq. (9) through any cross sectional area of the micro/nanochannel system. In Eq. (9), the terms on the right-hand side are currents due to ion electromigration, diffusion, and convection, respectively.

All governing equations were written in a cylindrical coordinate system (r, θ, z). Utilizing the symmetry in the θ coordinate, we can recast the problem as an axisymmetric two-dimensional model (r, z). Because of the geometrical symmetry, the computational domain is taken as half the physical domain, as shown in Fig. 1b. Based on the physical model described in Fig. 1a, the boundary conditions required to solve Eqs. (2–8) are specified as follows:

Boundary AB:

$$\psi = 0, \quad \phi = \phi_1, \quad c_i = c_0, \quad p = 0. \tag{10a}$$

Boundaries BC and FG:

$$\frac{\partial \psi}{\partial r} = \frac{\partial \phi}{\partial r} = \frac{\partial c_i}{\partial r} = 0, \quad \vec{V} = 0. \tag{10b}$$

Boundaries CD and EF:

$$\frac{\partial c_i}{\partial z} = \frac{\partial \phi}{\partial z} = 0, \quad \vec{V} = 0, \quad \frac{\partial \psi}{\partial z} = -\frac{\sigma_L}{\varepsilon\varepsilon_0} \quad \text{for CD}, \quad \frac{\partial \psi}{\partial z} = -\frac{\sigma_R}{\varepsilon\varepsilon_0} \quad \text{for FE}. \tag{10c}$$

Boundary DE:

$$\frac{\partial \phi}{\partial r} = 0, \quad \vec{V} = 0, \quad \frac{\partial \psi}{\partial r} = -\frac{\sigma_{\text{ch}}}{\varepsilon\varepsilon_0}, \quad \frac{\partial c_i}{\partial r} = 0. \tag{10d}$$

Boundary GH:

$$\psi = 0, \quad \phi = \phi_2, \quad c_i = c_0, \quad p = 0. \tag{10e}$$

Boundary AH:

$$\frac{\partial \psi}{\partial r} = \frac{\partial \phi}{\partial r} = \frac{\partial c_i}{\partial r} = \frac{\partial \vec{V}}{\partial r} = 0. \tag{10f}$$

4 Numerical model

Equations (2–8) along with the boundary conditions given in Eq. (10) were solved using the commercial code COMSOL 4.1 (http://www.comsol.com/). The finite element calculations were performed using quadratic triangular elements. Since the numerical accuracy depends strongly on the mesh size, a refined mesh is necessary in the regions near the charged channel wall, entrance, and exit where the dependent variable gradients are pronounced. A finer mesh was used in these regions for capturing the subtle changes in ion concentration, fluid flow, and electrical potential. Solution independence of the mesh size was carefully studied before reporting the final results. Moreover, the current was computed using the weak constraints provided by the COMSOL. Accurate ionic flux can be obtained by solving the Lagrange multipliers along with the governing equations.

5 Results and discussion

KCl aqueous solutions at $T = 298$ K were used as the working fluid. The dielectric constant of the KCl aqueous solution is 80, the molecular diffusivities of K^+ and Cl^- are 1.96×10^{-9} and 2.03×10^{-9} m^2 s^{-1}, respectively. The density and viscosity of the solution are assumed to be 1,000 kg m^{-3} and 10^{-3} Pa s, respectively. The bulk concentration c_0 is chosen in the range of 10^{-5}–1 M. The nanochannel radius and length are fixed as 25 nm and 1 μm, respectively. The microchannel length L_R is fixed at 3 μm while the radius varies in the range of 0.25–1.5 μm. From the literature, the nanochannel wall surface charge density depends on the channel material, pH value, and ionic strength of the bulk electrolyte [32, 33]. In this study, σ_{av} is chosen in the range from -1×10^{-3} to -5×10^{-3} C m^{-2} in order to obtain a reliable numerical solution. The parameter that specifies the channel surface charge density slope A is chosen in the range from -1.5 to 0. Using $\sigma_{\text{av}} = -1 \times 10^{-3}$ C m^{-2}, typical σ_{ch} variations are shown in Fig. 2. For $A = -1.5$, it is seen that σ_{ch} near the right end of the nanochannel has a positive value while σ_{ch} for the remainder of the nanochannel has a negative value. This arrangement is similar to that in the nanofluidic diode except that the surface charge density varied linearly [34]. For the neutral sidewalls (NS), both σ_L and σ_R are equal to zero. For the charged sidewalls (CS), the surface charge densities are assigned as $\sigma_L = \sigma_{\text{ch}}(-L/2) = (1 - A)\sigma_{\text{av}}$ and $\sigma_R = \sigma_{\text{ch}}(L/2) = (1 + A)\sigma_{\text{av}}$, respectively. That is the sidewall is treated as an extension of the nanochannel wall.

We first validated our numerical model by comparing the predicted nanochannel conductance with that predicted using a simple model proposed by Schoch and Renaud [35] using aqueous KCl solution as the electrolyte. For a negatively charged nanoslit, Schoch and Renaud [35] provided a simple model to describe the charged nanoslit conductance based on the effective surface charge density. For a cylindrical nanochannel, this model can be rewritten as,

$$G = F^2 c_0 \frac{\pi a^2}{L}(m_{K^+} + m_{Cl^-}) + F^2 m_{K^+} c_e \frac{2\pi a^2 |\sigma_{\text{ch}}|}{LF}. \tag{11}$$

In Eq. (11), G is the nanochannel conductance, m_{K^+} and m_{Cl^-} are the electric mobilities of K^+ and Cl^-,

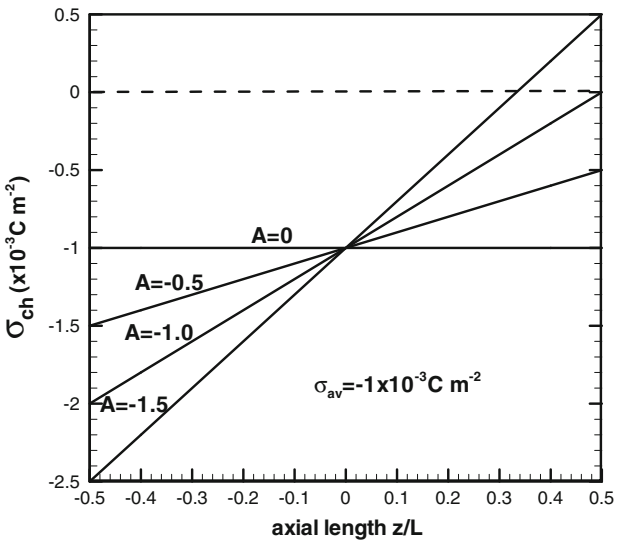

Fig. 2 Nanochannel surface charge density variation as function of nanochannel length and slope parameter A

respectively. For a uniformly charged nanochannel with $\sigma_{ch} = \sigma_{av} = \sigma_L = \sigma_R = -1 \times 10^{-3}$ C m^{-2}, the comparison between the nanochannel conductance predicted from the present numerical model and from the simple model described in Eq. (11) is shown in Fig. 3. It is seen that the agreement is good. Based on this comparison, it is believed that our model is correct and can be extended to ionic transport in a nanochannel with CS and a non-uniformly distributed wall surface charge density.

Figure 4 shows the typical *I–V* curves for a micro/nanochannel system under various surface charge density distributions. The parameters used are $c_0 = 10^{-4}$ M, $\sigma_{av} = -1 \times 10^{-3}$ C m^{-2}, and $b = 0.25$ μm. For the $|\Delta\phi|$ chosen in the range of 0–2 V, Fig. 4 shows the nanochannel with CS can affect the ionic current significantly compared to the nanochannel with NS. For the uniformly charged nanochannel ($A = 0$) shown in Fig. 4a, the *I–V* curves are symmetrical with respect to the applied voltage, which indicates that no current rectification can be obtained. For the CS case, more counterions (K^+) can be attracted into the nanochannel entrance and exit regions and transported through the nanochannel because both σ_L and σ_R have negative values. This results in higher ionic current. For the $A \neq 0$ cases, diode-like *I–V* behavior can be observed due to the asymmetric surface charge density variation along the nanochannel. Figure 4b–d shows that the ionic current increases with the increase in $|A|$ when positive voltage is applied. Similar to the $A = 0$ case, higher current can be obtained when the sidewall charge effect is included. For negatively applied voltage, ionic current decreases with the increase in $|A|$. That is the CS can enhance the ionic current rectification.

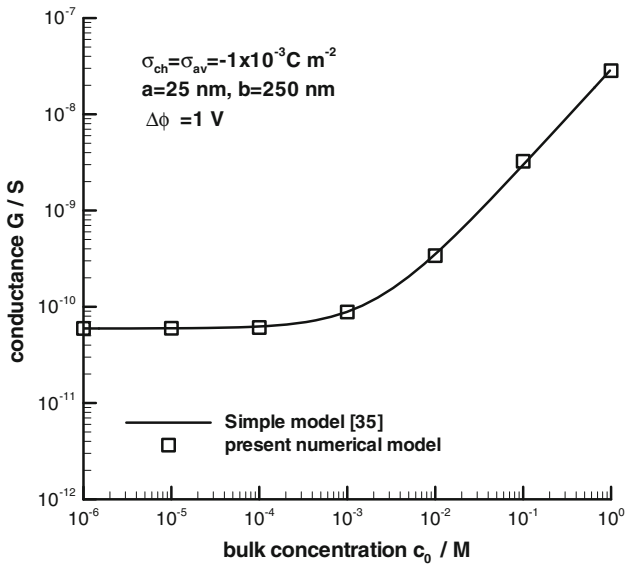

Fig. 3 Numerical model verification by comparing the numerically predicted nanochannel conductance with that predicted using the simple model proposed by Schoch and Renaud [35]

Another important observation from Fig. 4 is the slope variation in *I–V* curves as a function of the applied voltage. In the low applied voltage regime, the current varies linearly with the applied voltage obeying the Ohmic law. As shown in Fig. 4, the applied voltage regime for the Ohmic *I–V* relation is in the range of $|\Delta\phi| < 0.5$ V. In this low applied voltage regime, the sidewall charge effect on the *I–V* variation is not significant. The sidewall charge effect can be clearly identified when $|\Delta\phi| > 0.5$ V. For NS cases with positive applied voltage, the *I–V* curve has nearly zero slope similar to the limiting *I–V* relation observed in the charged permselective membrane [17, 18]. For the CS case, the limiting current cannot be observed in the *I–V* curve. Instead, he *I–V* curve varies approximately linearly with the larger slope compared to that in the Ohmic relation. In this study, the maximum applied voltage was chosen as 2 V because we intended to focus on the sidewall charge effect on ionic transport. It would be interesting to examine the *I–V* curve in the over-limiting current regime with higher applied voltage for the micro/nanochannel system considered in this study.

To have more understanding of the sidewall charge effect on ionic transport behavior, the ionic concentration distributions along the centerline of the micro/nanochannel system corresponding to the results shown in Fig. 4 are shown in Fig. 5. Figure 5 shows that the CS can promote concentration polarization. That is, a CS produces higher concentration gradient in the diffusion layer compared with the NS cases under the same applied voltage. Using Fig. 5a for the uniformly charged nanochannel ($A = 0$) as an example, zero ionic distribution can be obtained for the CS case while the ion concentration still drops linearly for the NS case under the same applied voltage. Similar ionic distribution can also be found for cases in which the nanochannel has linearly distributed surface charge densities, as shown in Fig. 5b–d. Figure 5 also shows that higher ionic concentration through the nanochannel is obtained as $|A|$ increases. In Fig. 6, the streamlines corresponding to Fig. 5 with $\Delta\phi = 1$ V are shown for both neutral and CS cases. A vortex structure forms at both the nanochannel entrance and exit. The size of the vortex structure is found to depend on the $|A|$ value and sidewall-charged condition. As shown in Fig. 6a, the vortex in the NS cases is limited to the micro/nanochannel junction corner with small size. In the CS cases, the vortex size increases with the $|A|$ value and occupies the entire nanochannel entrance region. The fluid stirring created by the vortex structure is related to the over-limiting current phenomena [21, 22]. In connection with the linear *I–V* relation for high applied voltage shown in Fig. 4, we may conclude that the inclusion of a CS produces no limiting current regime. That is, over-limiting current can be obtained directly when the applied voltage is >0.5 V for the micro/nanochannel system with CS.

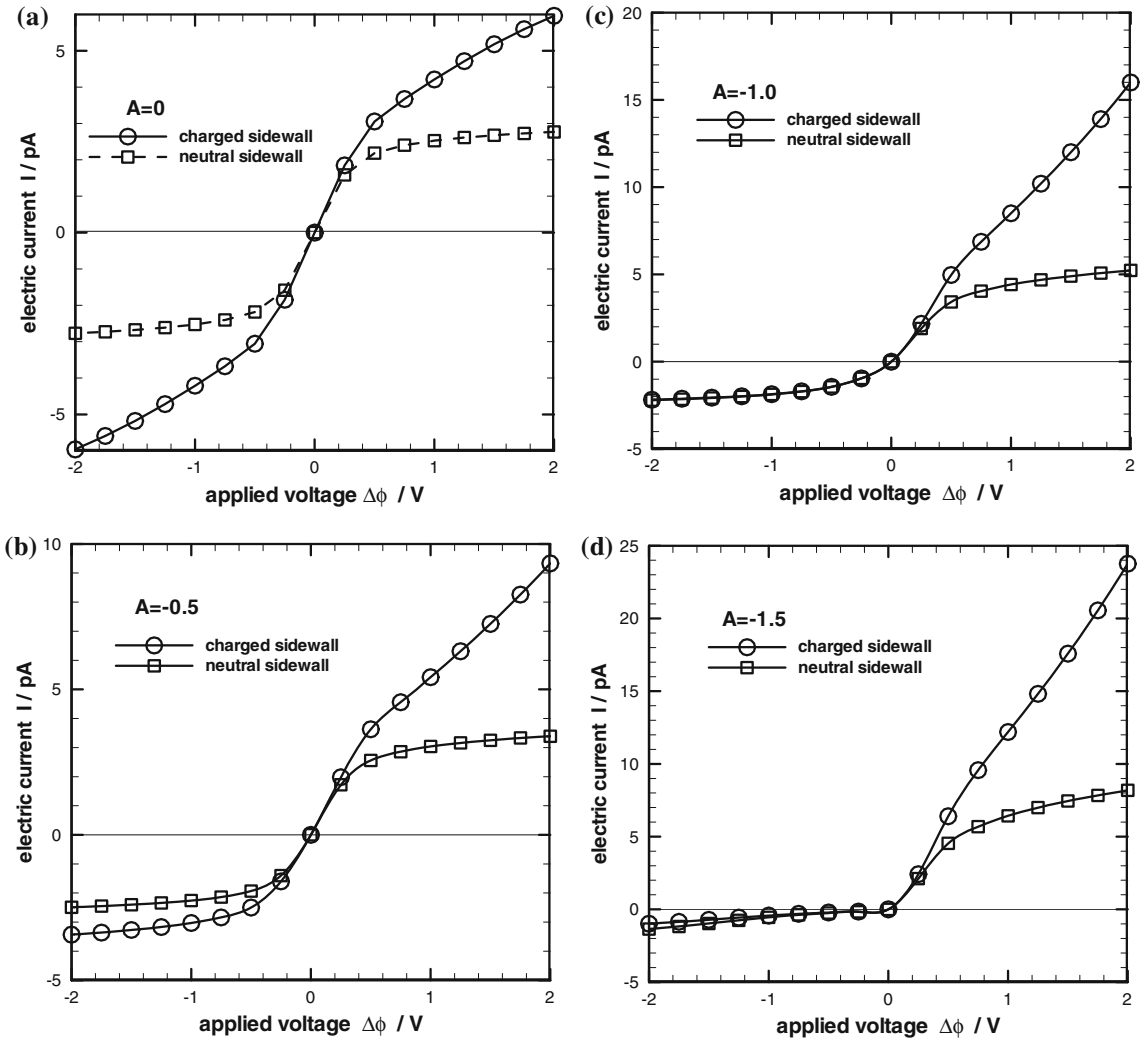

Fig. 4 *I–V* curve as functions of σ_{ch} variation and applied voltage for both nanochannels with neutral and CSs. $c_0 = 10^{-4}$ M, $\sigma_{av} = -1 \times 10^{-3}$ C m^{-2}, and $b = 0.25$ μm. **a** $A = 0$, **b** $A = -0.5$, **c** $A = -1.0$, and **d** $A = -1.5$

The ionic current rectification ratio can be computed from the *I–V* curves. The ionic current rectification ratio IR is defined as,

$$\mathrm{IR} = \frac{I(\Delta\phi)}{I(-\Delta\phi)}, \tag{12}$$

where $I(\Delta\phi)$ and $I(-\Delta\phi)$ are the ionic currents under the $\Delta\phi$ and $-\Delta\phi$ applied voltages, respectively. In Fig. 7, we examine the applied voltage effect on IR based on the results shown in Fig. 4. The CS effect on IR can be clearly seen in the high $\Delta\phi$ regime. For the NS with $A = -0.5$ and -1, it is seen that IR increases and reaches a saturation value as $\Delta\phi$ increases. For a CS with $A = -0.5$ and -1, IR varies linearly with the applied voltage and has higher value compared with the NS case. For the $A = -1.5$ case, the IR variation behavior is different from the $A = -0.5$ and -1 cases. For both neutral and CS cases, maximum IR values appear at $\Delta\phi = 0.5$ V. As noted earlier that the surface charge density near the nanochannel exit has a positive value for the $A = -1.5$ case while the entire nanochannel is negatively charged for the $A = -0.5$ and -1.0 cases. This difference leads to different IR variations as shown in Fig. 7.

A series of simulations were performed for c_0 varying in the $10^{-5} \sim 1$ M range to study the bulk concentration effect on the ionic transport through the micro/nanochannel system. Figure 8 shows the IR as functions of the c_0 and σ_{ch} variation under $\sigma_{av} = -1 \times 10^{-3}$ C m^{-2}, $b = 0.25$ μm, and $\Delta\phi = 1$ V conditions. For NS with $A = -0.5$ and -1.0, it is seen that IR increases with c_0 and reaches a maximum value at $c_0 = 10^{-3}$ M, and then decreases as c_0 increases. For the NS with $A = -1.5$, the value of c_0 at

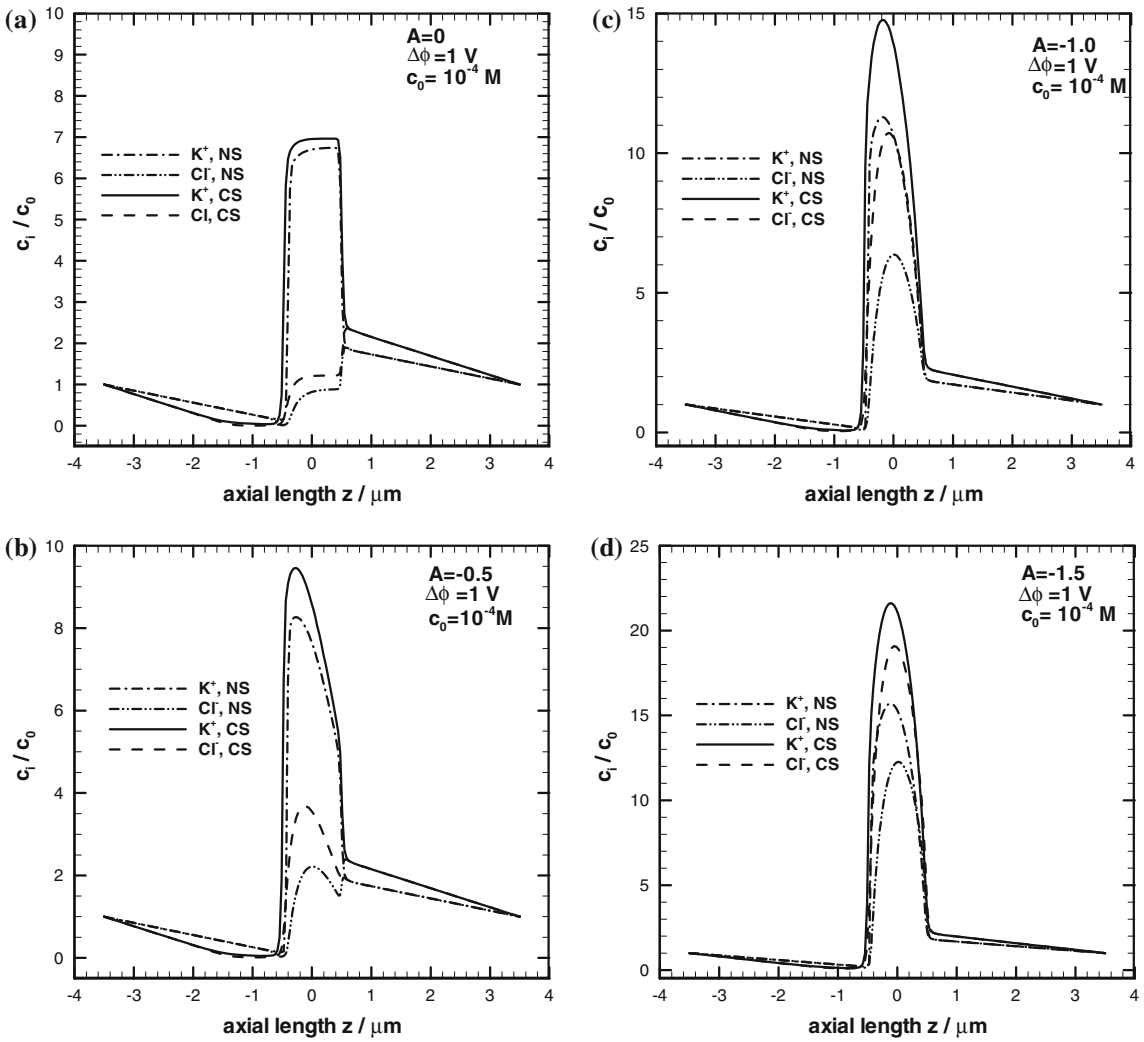

Fig. 5 Ionic concentration distributions along the centerline of the micro/nanochannel system corresponding to Fig. 4 with $\Delta\phi = 1$ V. **a** $A = 0$, **b** $A = -0.5$, **c** $A = -1.0$, and **d** $A = -1.5$

which the maximum IR occurs is 10^{-4} M because of the difference in σ_{ch} distributions. The existence of a maximum IR value as a function of the bulk concentration has been observed in many experimental measurements and theoretical analyses [36, 37]. Based on these studies, the maximum IR occurs with the bulk concentration at which nanochannel conductivity began to differ substantially from the electrolyte bulk conductivity. In our study, the nanochannel wall has a linearly varied surface charge density distribution. For the NS case, the averaged surface charge density would be equal to σ_{av}. The nanochannel conductance is shown in Fig. 4 using $\sigma_{ch} = \sigma_{av} = -1 \times 10^{-3}$ C m^{-2}. The bulk concentration at which the nanochannel conductance began to change substantially from the bulk conductivity is about $c_0 = 10^{-3}$ M, which is the bulk concentration at which the maximum IR occurs for a nanochannel with a NS. For the CS with $A = -0.5$ and -1.0, the IR variations are similar to those of the NS except with the higher values. For $A = -1.5$, the IR increases with the decreasing bulk concentration. Again, this is due to the different σ_{ch} distributions among $A = -0.5$, -1, and -1.5.

For the proposed micro/nanochannel system, the sidewall size is determined by the microchannel radius. Using the microchannel radius to characterize the sidewall size, we examined the sidewall size effect on the IR as a function of the bulk concentration and surface charge density variations under the $A = -1.5$ and $\sigma_{av} = -1 \times 10^{-3}$ C m^{-2} conditions with the results shown in Fig. 9. The sidewall size effect on IR is not significant in the high bulk concentration regime for both the nanochannels with neutral and CS. In the low bulk concentration regime, IR is found

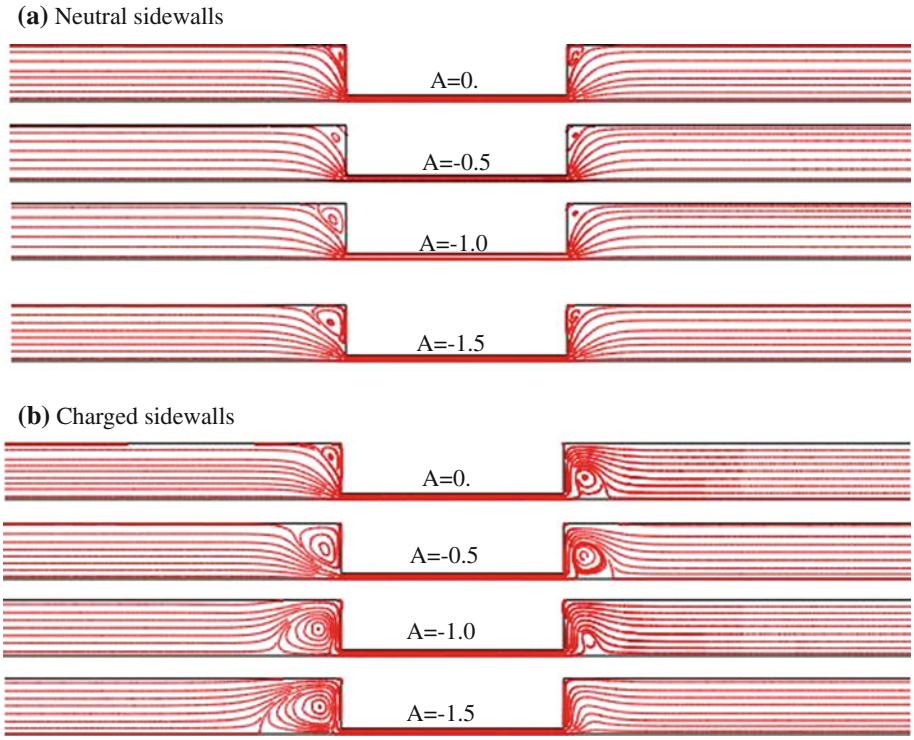

Fig. 6 Streamlines in the micro/nanochannel system. The numerical parameters are the same as those used in Fig. 4 and the applied voltage is $\Delta\phi = 1$ V. The anode is on the *left-hand side* while the cathode is on the right-hand side. **a** NS and **b** CS

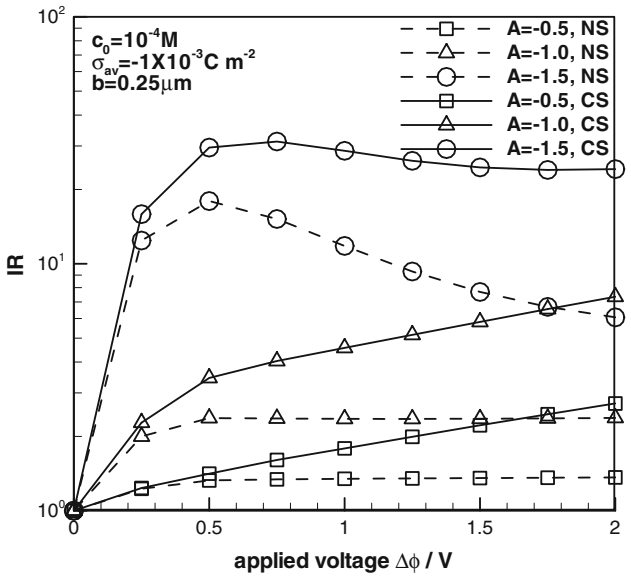

Fig. 7 Ionic current rectification ratio IR as functions of applied voltage and σ_{ch} variation

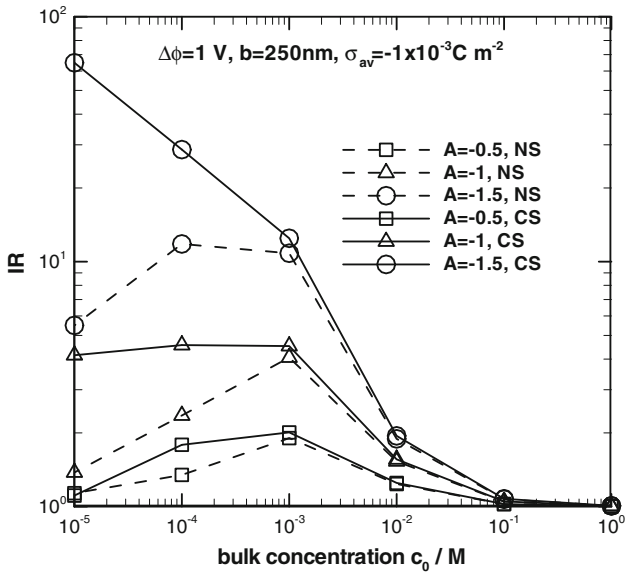

Fig. 8 Ionic current rectification ratio IR as function of the bulk concentraion and σ_{ch} variation. $b = 0.25$ μm

to increase with the decreasing bulk concentration and increasing sidewall size. For the NS cases, maximum IR occurs at $c_0 = 10^{-4}$ M for the same reason described above. For the CS cases, increasing sidewall length implies that more counterions will be attracted into the entrance and exit regions of the nanochannel. As a result, IR increases as the bulk concentration decreases without a maximum value.

We finally examined the surface charge density magnitude effect on the IR of the micro/nanochannel system. In Fig. 10, σ_{av} varies in the range from -1×10^{-3} to -5×10^{-3} C m^{-2} while b, $\Delta\phi$ and A are fixed as 1 μm, 1 V, and −1.5. Because more counterions are required to balance the surface charge, Fig. 10 indicates that high IR can be obtained with higher surface charge density magnitude for both nanochannels with neutral and CS.

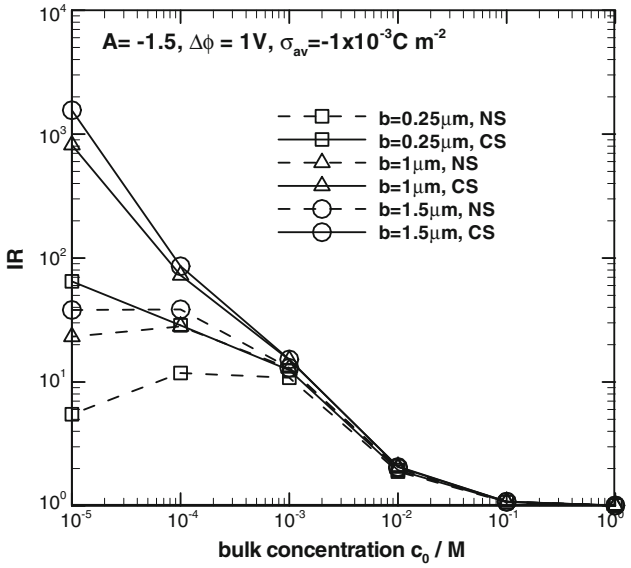

Fig. 9 Ionic current rectification ratio IR as function of the bulk concentration and sidewall length b. $A = -1.5$, $\Delta\phi = 1$ V, $\sigma_{av} = -1 \times 10^{-3}$ C m^{-2}

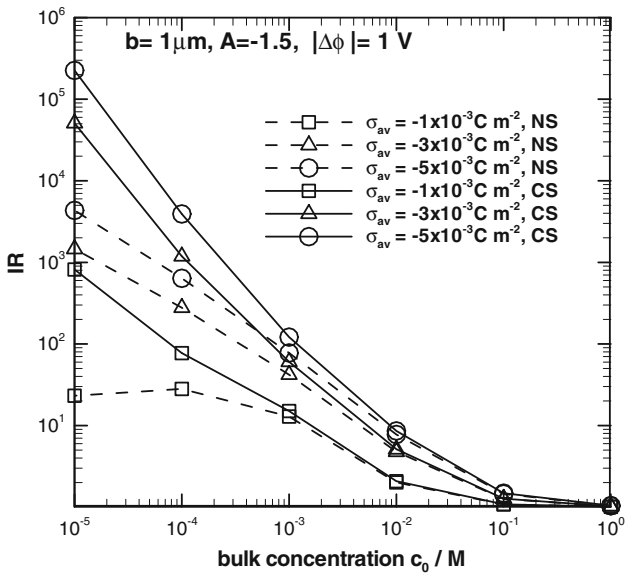

Fig. 10 Ionic current rectification ratio IR as function of the bulk concentration and σ_{ch} variation. $A = -1.5$, $b = 1$ μm, $\Delta\phi = 1$ V

6 Conclusions

This study examined the sidewall-charged condition on the ionic transport characteristics in micro/nanochannel systems with linearly varied surface charge density distribution. The following conclusions are made based on the numerical results obtained in this study:

(1) When the sidewall is charged, more counterions are attracted into the regions near the nanochannel entrance and exit. As voltage is applied, higher ionic current results compared to the nanochannel with NSs.

(2) The *I–V* relation of the micro/nanochannel system depends on both the sidewall-charged condition and nanochannel surface charge density distribution. With low applied voltage, the *I–V* curve obeys the Ohmic law having a linear relation. The sidewall-charged condition effect in this applied voltage regime is not significant. In a high applied voltage regime, a limiting current phenomenon similar to that in a permselective membrane can be found for the nanochannel with NS. For the nanochannel with CS, it was found that there is no limiting current in the *I–V* relation. Instead a linear *I–V* curve with slope higher than the Ohmic *I–V* relation is obtained. That is, there is no limiting current regime in the *I–V* curve for the nanochannel with CS and the *I–V* curve is in the over-limiting regime.

(3) For the linearly distributed surface charge density with higher slopes, diode-like *I–V* behavior can be found for both nanochannels with neutral and CS. For the NS cases, a maximum ionic current rectification ratio can be found at a certain bulk concentration similar to that observed in conical nanopores. For the CS cases, there is no maximum ionic rectification ratio occurring at a certain bulk concentration. The ionic current rectification ratio was found to increase with the slope of the linear surface charge density distribution, averaged surface charge density magnitude, and sidewall size.

References

1. Abgrall P, Nguyen NT (2008) Nanofluidic devices and their applications. Anal Chem 80(7):2326–2341
2. Schoch R, Han J, Renaud P (2008) Transport phenomena in nanofluidics. Rev Mod Phys 80:839–883
3. Pu Q, Yun J, Temkin H, Liu S (2004) Ion-enrichment and ion depletion effect of nanochannel structures. Nano Lett 4:1099–1103
4. Vlassiouk I, Smirnov S, Siwy Z (2008) Ionic selectivity of single nanochannels. Nano Lett 8(7):1978–1985
5. Siwy Z (2006) Ion-current rectification in nanopores and nanotubes with broken symmetry. Adv Funct Mater 16:735–746
6. Wang Y, Pant K, Chen Z, Wang G, Diffey W, Ashley P, Sundaram S (2009) Numerical analysis of electrokinetic transport in micro-nanofluidic interconnect preconcentrator in hydrodynamic flow. Microfluid Nanofluidics 7:683–696
7. Ko SH, Song YA, Kim SJ, Kim M, Han J, Kang KH (2012) Nanofluidic preconcentration device in a straight microchannel using ion concentration polarization. Lab Chip 12:4472–4482
8. Napoli M, Eijkel JCT, Pennathur S (2010) Nanofluidic technology for biomolecule applications: a critical review. Lab Chip 10:957–985
9. Paik KH, Liu Y, Tabard-Cossa V, Waugh MJ, Huber DE, Provine J, Howe RT, Dutton RW, Davis RW (2012) Control of DNA capture by nanofluidic transistors. ACS Nano 6:6767–6775

10. Karnik R, Fan R, Yue M, Li D, Yang P, Majumdar A (2005) Electrostatic control of ions and molecules in nanofluidic transistors. Nano Lett 5:943–948
11. Daiguji H (2010) Ion transport in nanofluidic channels. Chem Soc Rev 39:901–911
12. Karnik R, Duan C, Castelino K, Daiguji H, Majumdar A (2007) Rectification of ionic current in a nanofluidic diode. Nano Lett 7:547–551
13. Guan W, Fan R, Reed MA (2011) Field-effect reconfigurable nanofluidic ionic diodes. Nat Commun 2:506. doi:10.1038/ncomms1514
14. Liu S, Pu Q, Gao L, Korzeniewski C, Matzke C (2005) From nanochannel-induced proton conduction enhancement to a nanochannel-based fuel cell. Nano Lett 5:1389–1393
15. Gillespie D (2012) High energy conversion efficiency in nanofluidic channels. Nano Lett 21:1410–1416
16. Hlushkou D, Perry JM, Jacobson SC, Tallarek U (2012) Propagating concentration polarization and ionic current rectification in a nanochannel/nanofunnel device. Anal Chem 84:267–274
17. Kalman EB, Sudre O, Vlassiouk I, Siwy ZS (2009) Control of ionic transport through gated single conical nanopores. Anal Bioanal Chem 394:413–419
18. Cheng LJ, Guo LJ (2007) Rectified ion transport through concentration gradient in homogeneous silica nanochannels. Nano Lett 7:3165–3171
19. Kim SJ, Wang Y, Lee JH, Jang H, Han J (2007) Concentration polarization and nonlinear electrokinetic flow near a nanofluidic channel. Phys Rev Lett 99:044501
20. Strathmann H (2011) Introduction to membrane science and technology. Wiley, Weinheim
21. Zaltzman B, Rubinstein IJ (2007) Electro-osmotic slip and electroconvective instability. J Fluid Mech 579:173–226
22. Chang HC, Yossifon G, Demekhin EA (2012) Nano-scale electrokinetics and micro-vortices: how micro-hydrodynamics affects nanofluidic ion flux. Annu Rev Fluid Mech 44:401–426
23. Aguilella-Arzo M, Aguilella VM, Eisenberg RS (2005) Computing numerically the access resistance of a pore. Euro Biophys J 34:314–322
24. Cheng LJ, Guo LJ (2010) Entrance effect on ion transport in nanochannels. Microfluid Nanofluidics 9:1033–1039
25. Kubeil C, Bund A (2011) The role of nanopore geometry for the rectification of ionic currents. J Phys Chem C 115:7866–7873
26. Masliyah JH, Bhattacharjee S (2006) Electrokinetic and colloid transport phenomena. Wiley, New York
27. Li D (2004) Electrokinetics in microfluidics. Elsevier Academic Press, Amsterdam
28. Ramirez P, Gomez V, Cervera J, Schiedt B, Mafe S (2007) Ion transport and selectivity in nanopores with spatially inhomogeneous fixed charge distributions. J Chem Phys 126:194703
29. Kosinska I, Goychuk I, Kostur M, Schmid G, Hanggi P (2008) Rectification in synthetic conical pores: a one-dimensional Poisson–Nernst–Planck model. Phys Rev E 77:31131
30. Qian S, Joo S, Ai Y, Cheney M, Hou W (2009) Effect of linear surface charged non-uniformities on the electrokinetic ionic current rectification in a conical nanopores. J Colloid Interface Sci 329:376–383
31. Probstein RF (1994) Physicochemical hydrodynamics: an introduction, 2nd ed. Wiley, New York
32. Behrens SH, Grier DG (2001) The charge of glass and silica surfaces. J Chem Phys 115:6716–6721
33. Cervera J, Schiedt B, Ramırez P (2005) A Poisson/Nernst–Planck model for ionic transport through synthetic conical Nanopores. Euro phys Lett 71:35–41
34. Vlassiouk I, Smirnov S, Siwy Z (2008) Nanofluidic ionic diodes comparison of analytical and numerical solutions. ACS Nano 2:1589–1602
35. Schoch R, Renaud P (2005) Ion transport through nano-slits dominated by the effective surface charge. Applied Phys Lett 86:253111
36. White HS, Bund A (2008) Ion current rectification at nanopores in glass membranes. Langmuir 24:2212–2218
37. Kovarik ML, Zhou K, Jacobson SC (2009) Conical nanopore diameter effect on ion current rectification. J Phys Chem B 113:15960–15966